




# Investigation DSC and XRD on the crystallization kinetics in the phosphate $\text{Li}_2\text{O}-\text{Li}_2\text{WO}_4-\text{TiO}_2-\text{P}_2\text{O}_5$ glassy ionic system

H. Es-Soufi<sup>1,2,\*</sup> , L. Bih<sup>1,3</sup>, Alan R. F. Lima<sup>4</sup>, A. El Bouari<sup>5</sup>, B. Manoun<sup>6</sup>, and S. Hussain<sup>7</sup>

<sup>1</sup>Equipe Physico-Chimie de la Matière Condensée, PCMC, Faculté des Sciences de Meknès, Université Moulay Ismail, Meknès, Morocco

<sup>2</sup>Ecole Supérieure de Génie Civil et des Nouvelles Technologies, Avenue Moulay Idriss II RUE KIFA No 38 V.N, 50003 Meknès, Morocco

<sup>3</sup>Département matériaux et procédés, ENSAM Meknès, Université Moulay Ismail, Meknès, Morocco

<sup>4</sup>Center of Nature Sciences, Federal University of São Carlos, Rod. Lauri Simões de Barros km 12, Buri, SP 18290-000, Brazil

<sup>5</sup>Laboratory of Physico-chemical of Applied Materials, Faculty of Sciences Ben M'Sik, Hassan II University, Casablanca, Morocco

<sup>6</sup>Laboratoire des Sciences des Matériaux, des Milieux et de la Modélisation (LS3M), Univ Hassan 1er, 26000 Khouribga, Morocco

<sup>7</sup>School of Materials Science and Engineering, Jiangsu University, Zhenjiang 212013, China

Received: 23 January 2021

Accepted: 9 August 2021

Published online:  
29 August 2021

© The Author(s), under exclusive licence to Springer Science+Business Media, LLC, part of Springer Nature 2021

## ABSTRACT

Solid electrolytes-based lithium phosphates have achieved a great evolution due to the safety problem in the lithium-ion battery. This work targets to investigate the prepared glasses within the  $20\text{Li}_2\text{O}-(50-x)\text{Li}_2\text{WO}_4-x\text{TiO}_2-30\text{P}_2\text{O}_5$  system, with  $0 \leq x \leq 15$  mol%. The bonds constituting the framework of these glasses were studied by Raman spectroscopy. The data analysis of the chemical durability showed that the dissolution rates depend on the composition of each glass. Thermal analysis by using the DSC technique was used to determine the activation energy of crystallization, it is found in the glassy composition ( $x = 5$ ) that  $E_c = 184.482$  kJ/mol. The determinate Avrami parameter is around 1.7, which allows suggesting the mechanism is surface crystallization. The crystallization process of the prepared glasses is carried out by heating samples at a suggested value of temperature around 550 °C for 4 and 12 h, with heating rate of 10 °C/min. The crystallized phases are identified by XRD. The results of the X-ray diffraction analysis confirm that  $\text{TiO}_2$  acts mainly as network forming units. The crystalline phases  $\text{Li}_2\text{WO}_4$  and  $\text{Li}_4\text{P}_2\text{O}_7$  are formed during the crystallization process. The formation of these crystalline phases into the glasses depends on the time of heating at a fixed crystallization temperature. FTIR spectra of the glass-ceramics show nearly the same IR vibrational modes likewise their parent glasses.

Address correspondence to E-mail: hichamessoufi@gmail.com

<https://doi.org/10.1007/s10854-021-06804-7>

## 1 Introduction

Glasses and glass–ceramics-based phosphates have attracted the attention of many researchers due to their potential applications in technology, like solid electrolyte [1]. All-solid-state batteries using solid electrolytes are expected to have long battery life [2]. In general, chemical side reactions are inhibited in inorganic solid electrolytes as the lithium ions move through these typical electrolytes. As a result of this, all-solid-state batteries are potentially safer than conventional lithium-ion batteries [3]. Also, they are considered to be ideal batteries for electric vehicles and plug-in hybrid electric vehicles [4]. The solid electrolytes with lithium-ion conductivity are potentially investigated considering their use in power sources [5, 6]. Solid electrolytes-based phosphate materials are good candidates owing to their easy preparation, low melting point, wide glass-forming region, and simple composition [7, 8]. Consequently, in the last decades, scientists paid considerable attention to  $\text{Li}^+$  ion glassy electrolytes [9, 10].

As well known, the ionic glasses have a wide thermal stability window, but they tend to crystallize at certain temperatures ( $T_c$ ). For this reason, their direct uses affect the performance of the ionic devices during high-temperature applications [11, 12]. The glass–ceramics derived from glasses present lower conductivity than the parent glasses. This depends on the low ionic conductivity of the precipitated crystallites. Nevertheless, other glass–ceramics exhibit higher conductivity than the pristine glasses of the same compositions, for example, in  $\text{Ag}^+$  ion-conducting  $\text{AgI–Ag}_2\text{O–MoO}_3$  glasses. Also, glass–ceramics obtained from the glass  $\text{Li}_2\text{O–Al}_2\text{O}_3\text{–TiO}_2\text{–P}_2\text{O}_5$  system exhibited higher conductivity than the host glass matrix. Indeed, the high conductivity is attributed to the formation of the  $\text{LiTi}_2(\text{PO}_4)_3$  phase during crystallization [13]. There are many attempts to optimize ionic conductivity by stabilization the superionic  $\alpha$ -phase of ionic compounds in the glass matrix. The first successful attempt has been realized with the stabilization of  $\alpha$ - $\text{AgI}$  within the glass  $\text{AgI–Ag}_2\text{O–B}_2\text{O}_3$  system by rapid quenching. Exceptionally, at room temperature,  $\alpha$ - $\text{AgI}$  has been established in glass–ceramics of the  $\text{AgI–Ag}_2\text{O–B}_2\text{O}_3$  system, which resulted in high  $\text{Ag}^+$  ion conductivity of  $10^{-1} \Omega^{-1} \text{cm}^{-1}$  [14].

Solid electrolytes-based crystalline phosphate materials are widely investigated in all-solid-state

batteries, for example,  $\text{Li}_4\text{P}_2\text{O}_7$ . The XRD data analysis showed that  $\text{Li}_4\text{P}_2\text{O}_7$  crystallized in triclinic structure with space group P-1. The linking  $\text{LiO}_4$  with  $\text{P}_2\text{O}_7$  groups allows the formation of a framework with large voids [5]. In this framework,  $\text{Li}^+$  ions move easily; thus, high conductivity is obtained. In the literature, it reported that  $\text{Li}_4\text{P}_2\text{O}_7$  has a rather high conductivity ( $\sim 10^{-1} \text{ s/m}$  at 925 k) [15]. Kartini et al. studied  $\text{Li}_4\text{P}_2\text{O}_7$  in the  $\text{Li}_4\text{P}_2\text{O}_7\text{–Li}_3\text{PO}_4$  composite with the highest content of 93.56 %  $\text{Li}_4\text{P}_2\text{O}_7$ . This composite achieved high ionic conductivity of  $3.85 \times 10^{-5} \text{ s/m}$  at room temperature. This ionic conductivity is higher in comparison to the single phase of  $\text{LiPO}_3$ ,  $\text{Li}_3\text{PO}_4$ , and  $\text{Li}_4\text{P}_2\text{O}_7$ . As a result of this, the composite  $\text{Li}_4\text{P}_2\text{O}_7\text{–Li}_3\text{PO}_4$  is a good solid electrolyte for all-solid-state batteries [16].

Another example,  $\text{Li}_2\text{WO}_4$  compound crystallized in the monoclinic structure with space group (P2/m) and the lattice parameters:  $a = 9.753 \text{ \AA}$ ,  $b = 5.954 \text{ \AA}$ ,  $c = 4.994 \text{ \AA}$ ,  $\alpha = \gamma = 90^\circ$ , and  $\beta = 96.81^\circ$ . A structural study showed that the presence of some porosity is observed [17]. The presence of porosity is very important for  $\text{Li}^+$  ions to move into the  $\text{LiWO}_4$  structure. The electrical conductivity was carried out in the [200–500 °C] temperature range. The electrical measurements showed the  $\text{Li}^+$  ion conductivity is about  $2.18 \times 10^{-7} \text{ s/cm}$  at 300 °C, and the activation energy is 0.94 eV [18]. The  $\text{Li}_2\text{WO}_4$  and  $\text{Li}_4\text{P}_2\text{O}_7$  ionic conductors have also been reported to exhibit electrical conductivity. Nevertheless, according to our best knowledge, there is no work dealing with the  $\text{Li}_2\text{WO}_4\text{–Li}_4\text{P}_2\text{O}_7$  compound. Our attempts focused on precipitating  $\text{Li}_2\text{WO}_4$  and  $\text{Li}_4\text{P}_2\text{O}_7$  crystallites in  $\text{Li}_2\text{O–Li}_2\text{WO}_4\text{–TiO}_2\text{–P}_2\text{O}_5$  glasses [18]. The precipitation of these crystallites would greatly enhance the ionic conductivity of glass–ceramics. This study was performed to stabilize single or more crystalline phases already known for their high ionic conductivity.

The aim of the work is to investigate the prepared glasses within the  $\text{Li}_2\text{O–Li}_2\text{WO}_4\text{–TiO}_2\text{–P}_2\text{O}_5$  system. Their characterization was carried out by Raman spectroscopy and chemical durability tests. The crystallization kinetic study was performed by using thermal analysis. The glass–ceramics are characterized by X-ray diffraction and Infrared spectroscopy (IR).

## 2 Experimental procedure

### 2.1 Samples preparation

The phosphate glasses of the  $20\text{Li}_2\text{O}-(50-x)\text{Li}_2\text{WO}_4-x\text{TiO}_2-30\text{P}_2\text{O}_5$  system ( $x = 0, 5, 8, 10,$  and  $15$  mol%) were prepared from the raw materials (purchased from Sigma–Aldrich, USA): lithium carbonate ( $\text{Li}_2\text{CO}_3$ ), titanium trioxide ( $\text{TiO}_2$ ), lithium tungstate  $\text{Li}_2\text{WO}_4$ , and hydrogen ammonium phosphate ( $\text{NH}_4\text{H}_2\text{PO}_4$ ). The detailed experimental protocol of preparing glasses was described in our previous work [18]. The amorphous state of these colorless glasses was verified by XRD and confirmed by Raman spectroscopic analysis. Glassy samples were subjected to controlled thermal heat treatment through two-step regime. The glasses were heat treated at a rate of  $10\text{ }^\circ\text{C}/\text{min}$  to reach at temperature around  $550\text{ }^\circ\text{C}$  for 4 h and 12 h, sufficient to provide sufficient nucleation sites. The experimental processes to obtain glass–ceramics have summarized according to the schematic diagram in Fig. 1. The Muffle Furnace (Model LT 9/12, Nabertherm, Italy) with the samples inside was switched off and then left to cool to room temperature at a rate of  $1\text{ }^\circ\text{C}/\text{min}$ . These specific temperatures were collected from DSC measurements. The obtained glass–ceramics were analyzed by an X-ray Diffractometer (Model D5000, Bruker, USA) in the range of  $2\theta$  from  $10^\circ$  to  $80^\circ$ . The X-ray data were analyzed by X'Pert High Score Plus software to identify the crystalline phases.

### 2.2 Raman spectroscopy

The structural properties of the prepared glasses were studied by Raman spectroscopy. The Raman data are obtained at room temperature by using spectrometer (Model T64000, Horiba, Germany). The spectra were measured in backscattering geometry, under excitation with He–Ne laser radiation ( $632.8\text{ nm}$ ) at a power of  $12\text{ mW}$ . The exposure time was  $3\text{ s}$ , the accumulated number was  $10$ , and the spectral slit width was  $1\text{ mm}$ .

### 2.3 Durability testing

Chemical durability test of the glasses is carried out to determine the dissolution rate in distilled water at  $25\text{ }^\circ\text{C}$ . The prepared blocks of the glasses were placed into a bottle full of distilled water with pH  $6.8$ . The

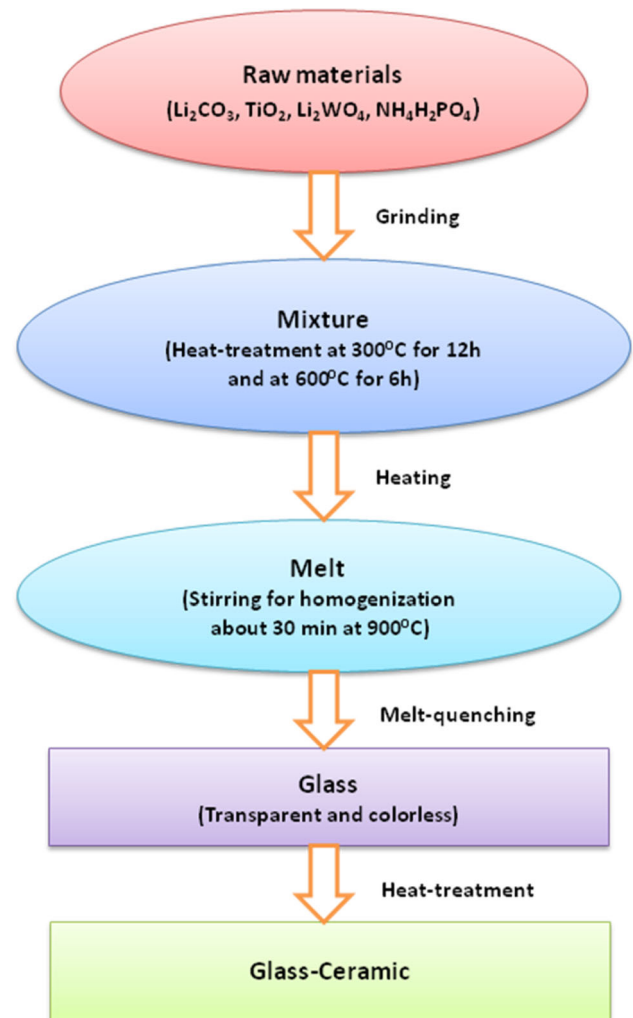


**Fig. 1** Schematic diagram for experimental protocol

bottles are suspended in an Electrical Thermostatic Water Bath (Model HH-420, BILON, China) kept at  $30\text{ }^\circ\text{C}$  for 250 h. The dissolution rate, DR, is calculated from the equation  $\text{DR} = \text{Dx}/(\text{S.t})$ , where Dx is the mass loss (g), S is the glass surface ( $\text{cm}^2$ ) before the dissolution test, and 't' is time of immersion (min). The pH value of leaching for each glass is measured every 24 h by a pH meter (Model Consort<sup>TM</sup> C3010, Thermo Fisher Scientific, USA).

### 2.4 Crystallization kinetics

The crystallization kinetics of the glasses is studied by differential scanning calorimetry (DSC). The fine grain powdered sample ( $< 50\text{ }\mu\text{m}$ ) of about  $40\text{ mg}$  was placed in an aluminum crucible and heated at a rate of  $5\text{ }^\circ\text{C}/\text{min}$ ,  $8\text{ }^\circ\text{C}/\text{min}$ ,  $10\text{ }^\circ\text{C}/\text{min}$ , and  $12\text{ }^\circ\text{C}/\text{min}$  using a DSC (Model 131 Evo analyzer, Thermo

Fisher Scientific, UK) from ambient temperature to 550 °C. The obtained data are investigated to determine the peak crystallization temperature ( $T_p$ ).

## 2.5 Infrared spectroscopy

The structural units formed the glass–ceramics were analyzed by a Fourier Transform Infrared (FTIR) spectrometer (Model Tensor 27, Bruker, UK). The IR spectra were recorded at room temperature in the frequency range (400–1500)  $\text{cm}^{-1}$ . The samples were ground to a fine powder and then mixed with KBr powder to prepare pellets for this study.

## 3 Results and discussion

### 3.1 Raman spectroscopy

Figure 2 presents the Raman spectra of the phosphate  $20\text{Li}_2\text{O}-(50-x)\text{Li}_2\text{WO}_4-x\text{TiO}_2-30\text{P}_2\text{O}_5$  glasses recorded in the wavenumber region 1200–150  $\text{cm}^{-1}$ . The band positions and their assignments are gathered in Table 1. The Raman spectra show different bands situated at different positions: 1055  $\text{cm}^{-1}$ , 930  $\text{cm}^{-1}$ , 870  $\text{cm}^{-1}$ , 740  $\text{cm}^{-1}$ , 635–510  $\text{cm}^{-1}$ , 372  $\text{cm}^{-1}$ , and 250  $\text{cm}^{-1}$ . The assignments of these bands were made by comparing with the literature data [19–24]. From the band positions, we divided the Raman spectra into the three wavenumber regions:

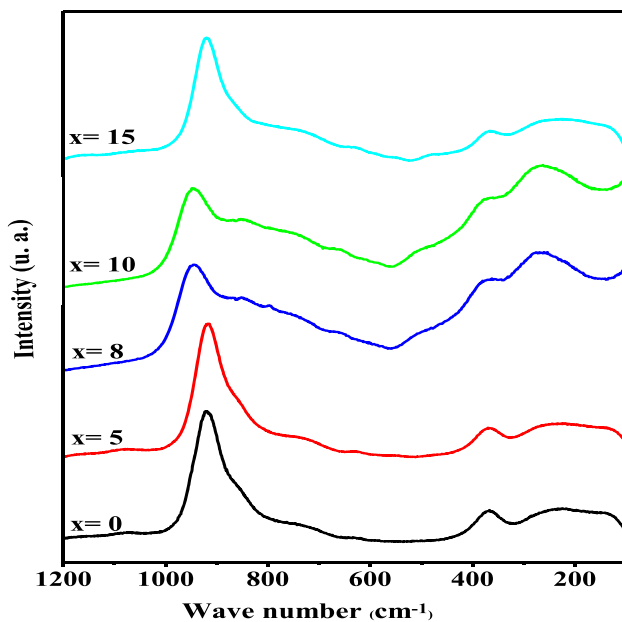


Fig. 2 Raman spectra of the studied glasses

- i) In the high wavenumber region, there is a band of low intensity at the position 1055  $\text{cm}^{-1}$ . This band is attributed to the asymmetric vibration  $\nu_{\text{as}}(\text{P-O}^-)$ ,  $\text{Q}^1$  units. The band at 930  $\text{cm}^{-1}$  of high intensity is assigned to the asymmetric vibration of the bond  $\text{P-O}^-$  into  $\text{Q}^0$  units or to the symmetric vibration  $\text{M-O}^-$  in a polyhedron with ( $\text{M} = \text{W}, \text{Mo}$ ).
- ii) For the intermediate region, a band the low intensity at 870  $\text{cm}^{-1}$  it observed associated with the symmetric vibration mode of the bond  $\text{W-O}$  bond of the  $\text{WO}_6$  polyhedron and/or  $\text{W-O-P}$  bond. Also, a band of low intensity is situated at the position 740  $\text{cm}^{-1}$  attributed to the symmetric vibration of the  $\text{P-O-P}$  bond of the  $\text{Q}^1$  unit.
- iii) In the low wavenumber region, the bands situated between 635 and 250  $\text{cm}^{-1}$  could be attributed to the stretching mode of the  $[\text{PO}_4]$  units.

After the substitution by  $\text{TiO}_2$  in the glassy composition ( $x = 5$ ), two supplementary bands are observed. These bands are situated around the positions 914  $\text{cm}^{-1}$  and 742  $\text{cm}^{-1}$  attributed to the  $\text{TiO}_4$  and  $\text{TiO}_6$ , respectively [25]. At  $\text{TiO}_2$  content increased, Raman spectra change, especially in the region of low frequencies. This shows that several structural units are present in the various networks. Besides, there is a considerable change in the intensity of the structural units of  $\text{TiO}_4$ . Such variations suggest that titanium ions occupy distorted octahedral positions and modify the vitreous matrix increasing the number of non-bridging oxygens (NBO). When  $\text{TiO}_2$  is present in larger quantities ( $x > 8$ ), the  $\text{P=O}$  bond can be broken by structural units of  $\text{TiO}_4$ , which can cause the creation of new

Table 1 Raman band assignments in the 1200–150  $\text{cm}^{-1}$  range frequency for the studied phosphate glasses

Position of band ( $\text{cm}^{-1}$ )	Band assignment
1055	$\nu_{\text{s}}(\text{PO}_2)^-$ , $\text{Q}^2$
930	$\nu_{\text{as}}(\text{P-O-P})/\nu_{\text{as}}(\text{P-O-M})$ ( $\text{M} = \text{W}, \text{Ti}$ )
870	$\text{O-Mo-O}/\text{MO}_4/\text{MO}_6$ ( $\text{M} = \text{W}, \text{Ti}$ )
740	$\nu_{\text{s}}(\text{P-O-P})$ , $\text{Q}^1$
635–510	$\nu_{\text{s}}(\text{P-O-P})$ , $\text{Q}^2$
372	$\nu_{\text{s}}(\text{M-O-M})$ ( $\text{M} = \text{W}, \text{Ti}$ )
250	$\delta \delta(\text{PO}_4)$

NBO ions facilitating the formation of structural units  $[\text{TiO}_{6/2}]^{2-}$  [26]. The analysis of Raman spectra shows that the degree of depolymerization of the glass lattice and the quality of  $\text{TiO}_6$  structural units increases with the increasing  $\text{TiO}_2$  content.

### 3.2 Chemical durability

#### 3.2.1 Weight loss

Chemical durability is expressed by the resistance of the glasses to attack chemical species found in a solution. This attack takes place through the process of ion exchange in the hydrated layer. When the chains are completely surrounded by water, they can separate from the partially hydrated chains and dissolve in solution. Once the hydrated layer is constant, the dissolution is linear over time [27].

Figure 3 represents the evolution of the weight loss at the initial surface ( $\text{g cm}^{-2}$ ) of the glass as a function of time (h). From Fig. 3, it is noted that the glasses present similar dissolution behavior. We can clearly differentiate two stages or two phases: (i)  $t < 100$  h, the dissolution is almost linear. (ii)  $100 \text{ h} < t < 250$ h, where the dissolution rate slows down. The substitution of  $\text{Li}_2\text{WO}_4$  by  $\text{TiO}_2$  has an observable effect on the dissolution behavior of the synthesized glasses. The dissolution of the glass ( $x = 0$  mol%) is characterized by an initial dissolution, faster than that of the other glass. The solubility of the studied glasses depends on the degree of substitution of  $\text{Li}_2\text{WO}_4$  by  $\text{TiO}_2$ . Indeed, the

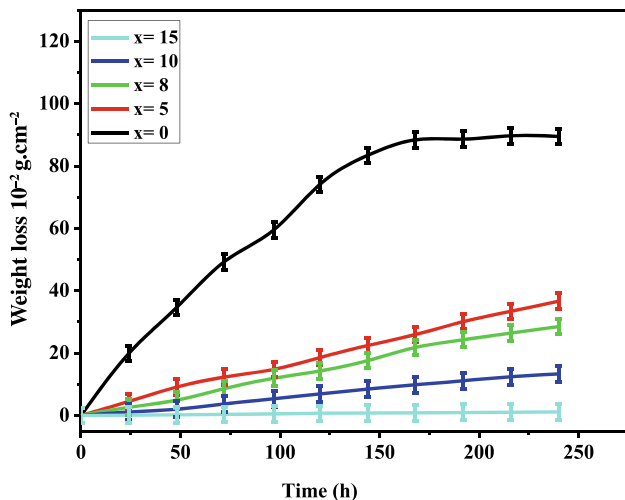


**Fig. 3** Evolution of the weight loss of the glasses as a function of time (h)

introduction of  $\text{TiO}_2$  in the glass network leads to improved chemical durability of the network. In our similar study, we reported that incorporating  $\text{Fe}_2\text{O}_3$  into the vitreous network leads to improve the chemical durability, which was explained by the formation of a new bond  $\text{P-O-Fe}$  in place of  $\text{P-O-P}$  [28]. By analogy,  $\text{TiO}_2$  also leads to the enhancement of the chemical durability of the network by the formation of bonds of the type  $\text{P-O-Ti}$ . These bonds are identified by Raman spectroscopy. These results agree with the thermal analysis, which showed that the introduction of  $\text{TiO}_2$  into the phosphate glass network makes the glass matrix harder.

The correlation between chemical durability and thermal analysis confirms that the introduction of  $\text{TiO}_2$  into the glass network leads to the strengthening of the chains, constituting the glass matrix of the  $\text{Li}_2\text{O-Li}_2\text{WO}_4\text{-TiO}_2\text{-P}_2\text{O}_5$  systems [29].

#### 3.2.2 pH variation

Figure 4 illustrates the evolution of the pH as a function of the immersion time in distilled water ( $\text{pH} \sim 6.8$ ) at a temperature of  $30^\circ\text{C}$ . The curves showed two zones: (i) before 48 h, there is a sudden decrease in pH curves; (ii) after 48 h, the pH value is almost constant. This variation in pH depends on the chemical composition of the glass. We can say that the alkali ions and the phosphate ions that constitute the glass surface have been released into the solution. This ion exchange plays a major role which that defines the acid-base character of the solution. In fact,

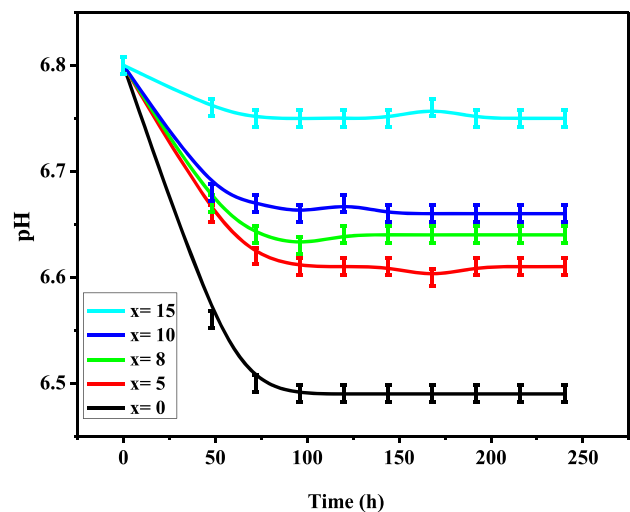


**Fig. 4** Evolution of the pH of the glasses as a function of time (h)



decreasing pH curves can be attributed to the disintegration of the phosphate entities. The variation of pH depends on the formation of phosphoric acid controlled by the entities  $\text{H}_2\text{PO}_4^-$  in water [30–33].

At  $\text{TiO}_2$  content increases, it is observed that the pH of the solution becomes smaller than the initial solution. These results indicate that the introduction of  $\text{TiO}_2$  into the glass network greatly improves chemical durability. In terms of this chemical study, it is believed that the corrosion mechanism of glasses occurs in two phases: (i) a rapid alteration phase where the thermodynamic imbalance between the glass and the altering solution is great, which creates a sudden decrease in pH; (ii) a corrosion slowing phase, which is associated with the saturation of the altering solution. This leads to the formation of a protective layer against diffusion through the surface of glass.

### 3.3 Crystallization kinetics by DSC

The crystallization kinetics have suggested calculating parameters of activation energy ( $E_c$ ) and Avrami exponent ( $n$ ). The activation energy ( $E_c$ ) of crystallization was calculated by using the following modified form of Kissinger Eq. (1), established by Matusita and Saka [34]:

$$\ln\left(\frac{T_p^2}{\beta}\right) = \frac{E_c}{(RT_p)} + \text{Constant}, \quad (1)$$

where  $\beta$ ,  $R$  and  $T_p$  are the heating rate, the universal gas constant (8.314 J/mol k), and the crystallization peak, respectively. Different heating rates  $\beta$  (5 °C/min, 8 °C/min, 10 °C/min, 12 °C/min) are deliberated to study the crystallization kinetics of the prepared glasses. The crystallization activation energy  $E_c$  is determinate to review the crystallization kinetics mechanism of glasses.

Figure 5 plots the DSC curves for the glassy composition  $x = 5$  mol% obtained at different heating rates  $\beta$ . The DSC curves present a broad crystallization peak shifted to high temperature, with an increase in the heating rate. The obtained crystallization temperature ( $T_p$ ) for the glass ( $x = 5$  mol%) is listed in Table 2. The plot of  $\ln(T_p^2/\beta)$  versus  $1/T_p$  is shown, a straight line is obtained (see Fig. 6), and from its slope, the value of  $E_c$  can be determined. The obtained value of the activation energy ( $E_c$ ) is 184.482 kJ/mol. This determinate activation energy

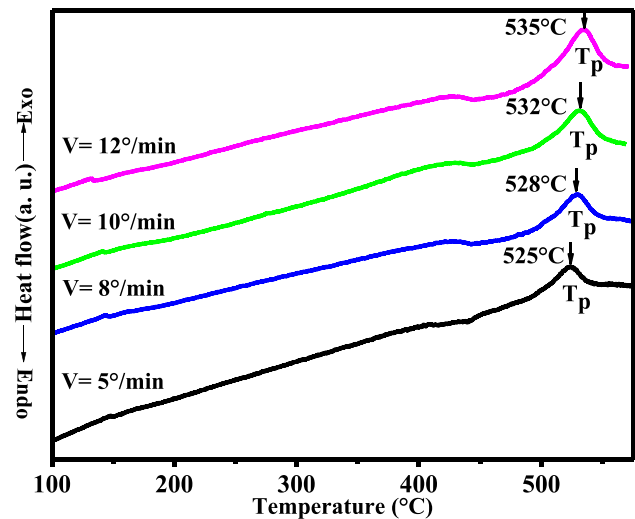


**Fig. 5** DSC curves for the glass ( $x = 5$ ) under different heating rates

**Table 2** Crystallization temperature of the glass ( $x = 5$  mol %) at different heat crystallization rates

Glass	$\beta$ (°C/min)	$T_p$	$\Delta T$	Avrami parameter ( $n$ )
$x = 5$	5	524	14	2.20
	8	528	16	1.96
	10	532	22	1.45
	12	534	25	1.28

relies on the bond energy of the glassy framework. In submitting a material to heat treatment, its weak bonds destroy. Remarkably, stable crystalline phases can be precipitated into heated glasses. The studied glassy network consists of the bonds Li–O, P–O, Ti–O, and W–O, respectively, their bond energies are 333.5 kJ/mol, 599 kJ/mol, 666.5 kJ/mol, and 720 kJ/mol [35]. At first glance, we bet on destroying the Li–O bonds, because it needs low energy in comparison with other bonds. Therefore, the crystallization of crystalline phases in the glass–ceramics is expected to the break of the Li–O bonds (see the section of the X-ray diffraction of glass–ceramics). Additionally, the crystallization kinetics mechanism could be clear by using the Avrami parameter  $n$  calculated by applying the Augis–Bennett Eq. (2) [36]:

$$n = \left(\frac{2.5}{\Delta T}\right) \times \left(\frac{RT_p^2}{E_c}\right), \quad (2)$$

where  $\Delta T$  is the full width of the exothermic DSC peak at the half-maximum intensity, and ( $n$ ) is the Avrami exponent or crystallization index. The

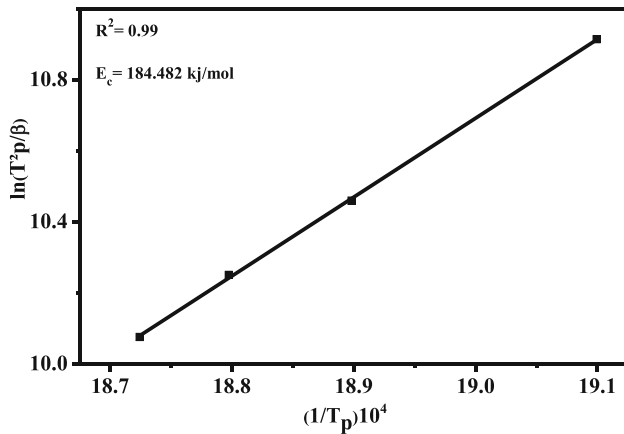


**Fig. 6** Plot of  $\ln(T^2 p/\beta)$  versus inverse temperature for the glass

Avrami exponent ( $n$ ) had indicated the nucleation and growth mechanism. According to the Johnson–Mehl–Avrami (JMA) theory, ( $n$ ) was also related to crystallization pattern,  $n = 2$  means that the surface crystallization dominates the overall crystallization,  $n = 3$  means two-dimensional crystallization,  $n = 4$  means that three-dimensional crystallization for bulk materials [37–39]. The value calculated for ( $n$ ) is very close to 1.7, suggesting that surface crystallization is dominant during the crystallization of the glasses [40, 41].

### 3.4 X-ray diffraction of glass–ceramics

From the DSC analysis, it has been suggested the crystallization temperature around 550 °C, as an average value of the analyzed glasses ( $x = 0, 5, 8, 10, 15$  mol%), where the crystallization temperature is picked at the maximum of the crystallization peak of each DSC curve. This temperature is determinate for the compositions  $x = 0$  mol% (about 503 °C) and  $x = 5$  mol% (around 532 °C). But, for the compositions  $x = 8, 10$ , and 15 mol%, the crystallization temperature is not determinate in the 500–575 °C region [18]. As a result of the treatment temperature, which fixed at 550 °C (suggested crystallization temperature), it has obtained glass–ceramics. The crystalline phases formed into heated glasses are identified by using X-ray diffraction. Figures 7 and 8 correspond to the X-ray patterns of glass–ceramics derived from the glasses of the  $20\text{Li}_2\text{O}-(50-x)\text{Li}_2\text{WO}_4-x\text{TiO}_2-30\text{P}_2\text{O}_5$  system, with  $0 \leq x \leq 15$  mol%. The X-ray patterns gathered in Fig. 7 showed the crystallization of crystalline phases into the compounds ( $x = 0$  and 5)  $\text{Li}_2\text{WO}_4$  (JCPDS# 01-072-0086)

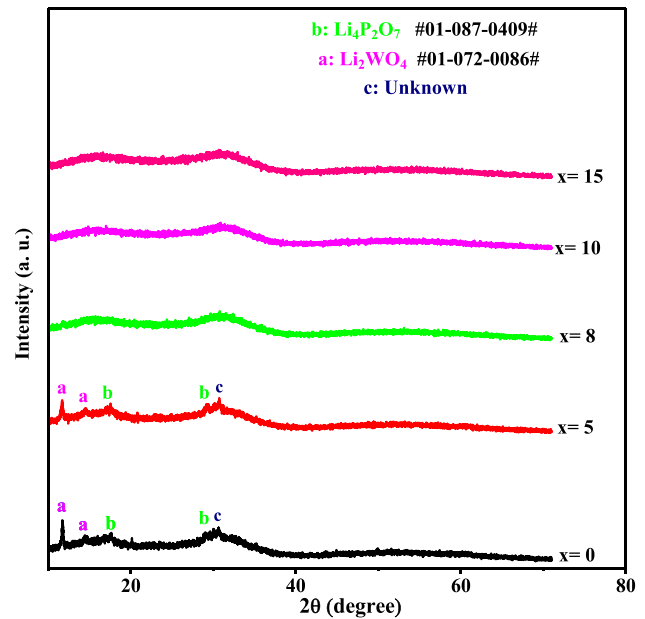


**Fig. 7** XRD patterns of the crystallized glasses at 550 °C for 4 h

and  $\text{Li}_4\text{P}_2\text{O}_7$  (JCPDS# 01-087-0409) during 4 h. These two formed crystalline phases are characterized by low intensity of the peaks. At high  $\text{TiO}_2$  content ( $x = 8, 10$ , and 15 mol%), it observed no crystalline phase formed. Nevertheless, at increasing the heating duration of 12 h, it observed that the intensity of the peaks is slightly increased in crystalline phases  $\text{Li}_2\text{WO}_4$  (JCPDS# 01-072-0086) and  $\text{Li}_4\text{P}_2\text{O}_7$  (JCPDS# 01-087-0409) for the compositions ( $x = 0$  and 5). But, in the compositions ( $x = 8, 10$ , and 15), there are peaks appeared which corresponding to the crystalline phases  $\text{Li}_4\text{P}_2\text{O}_7$  (JCPDS# 01-087-0409). According to the literature, the crystallographic data reported that the compound  $\text{Li}_2\text{WO}_4$  crystallized with monoclinic symmetry,  $C2c$ ,  $a = 9.753(1) \text{ \AA}$ ,  $b = 5.954(1) \text{ \AA}$ ,  $c = 4.994(1) \text{ \AA}$ ,  $\beta = 90.58(2)^\circ$ . In addition, the lithium and the tungsten atoms are located in octahedral sites. Furthermore, the structure is found in four octahedral layers parallel to (100). The first and the third layers are filled with lithium atoms, resulting in  $\text{LiO}_6$  octahedral sheets, while the second and the fourth contain zigzag chains of  $\text{WO}_6$  octahedral reported in the Wolframite structure [42]. Also, the compound of the crystal structure of  $\text{Li}_4\text{P}_2\text{O}_7$  was interpreted as triclinic, space group P-1, as confirmed by Voronin et al. [5]. As well known, the existing of titanium or tungsten ions in glass could play a double role: former in the glass of covalent  $[\text{MO}_4]$  groups ( $M = \text{Ti}, \text{W}$ ) and modifier in the ionic

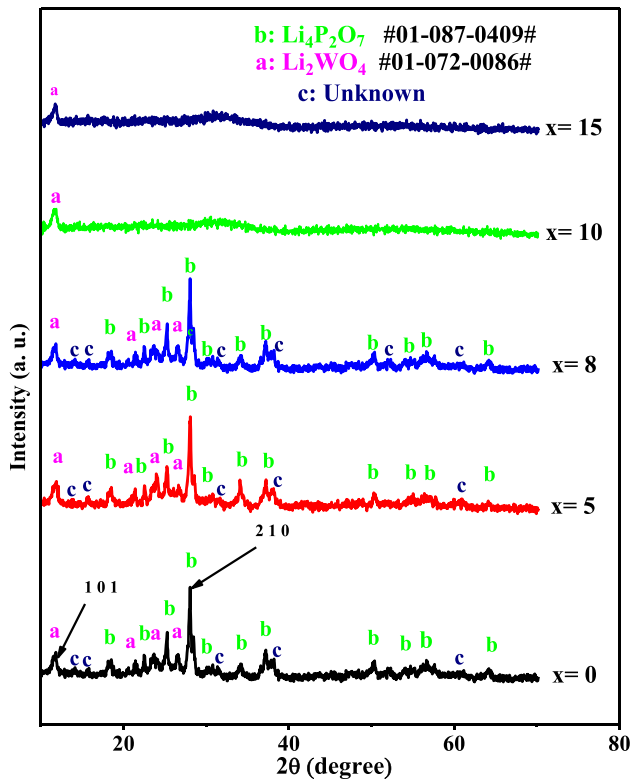


**Fig. 8** XRD patterns of the crystallized glasses at 550 °C for 12 h

glass of the  $[MO_6]$  polyhedrons.  $WO_3$  itself brings three oxygen atoms in  $[WO_{6/2}]$  structural units. On the other hand,  $TiO_2$  itself takes stoichiometrically two oxygen atoms in  $[TiO_{4/2}]$  and passing to six coordination. Therefore, the titanium atoms obtain oxygen from the glassy network. The determination of layer size is an important test for the characterization of heat-treated glasses.

The crystallite size values are estimated from X-ray patterns by using the Scherrer Eq. (3) [43]:

$$D = \frac{K\lambda}{\beta \cos \theta}, \quad (3)$$

where  $D$  is the average crystallite size,  $\lambda$  is the X-ray wavelength,  $\beta$  is the width of the X-ray peak on the  $2\theta$  axis, normally measured as full width at half maximum (FWHM),  $\theta$  is the Bragg angle, and  $K$  is the Scherrer constant with  $K = 0.9$ .  $K$  depends on the crystallite shape and the size distribution, indices of the diffraction line, and the actual definition used for  $\beta$  whether FWHM or integral breadth [44]. Since the exact value of  $K$  for the present materials system is not known, crystallite size calculations are only estimates. The calculated crystal sizes of the crystalline phases ( $Li_2WO_4$  and  $Li_4P_2O_7$ ) are given in Table 3,

where the crystal size of the  $Li_2WO_4$  is determined from the peak of the  $h, k, l$  value (1 0 1) and for  $Li_4P_2O_7$  was determined from the peak of the  $h, k, l$  value (2 1 0). From the measurements of the crystal size, it observed that the crystal size average is constant for each crystalline phase, where  $D_{(Li_2WO_4)} = 18$  nm and  $D_{(Li_4P_2O_7)} = 26$  nm. As the crystal size distribution and evolution during growth are well known, quantitative studies on the nucleation and growth of a fragment reveal that, with increasing growth time, both the crystal size and the size spectrum increase. During the early stages of growth, crystals are small and relatively uniform sized. As films grow, the average crystal size increases, and at the same time, the size distribution broadens. But the crystal size is independent of the diffraction peaks [45].

It seems that the vitreous network of glasses contains structural units of the pyrophosphate type. The crystallization times of the glasses for 4 and 12 h, insufficient for the formation of crystallized phases, contain the titanium, within the pieces of the heat-treated glass.

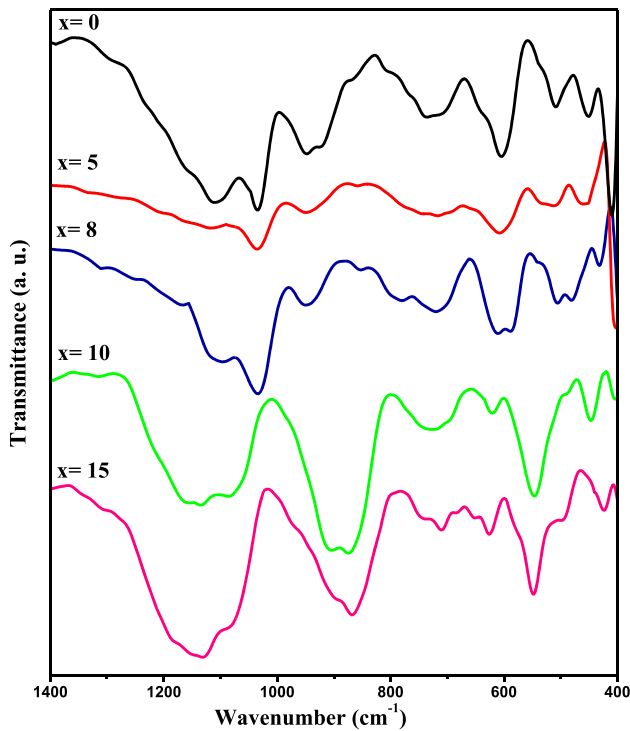
### 3.5 Infrared spectra of glass–ceramics

Figure 9 shows the IR spectra of the prepared glass–ceramics heated at 550 °C for 12 h. These spectra contain the same principal bands of the phosphate glasses with sharp differences between the glasses (previous work [18]) and their derived glass–ceramics. The spectra of the heat-treated glasses (glass–ceramics) show different absorption bands localized around  $1275\text{ cm}^{-1}$ ,  $1120\text{ cm}^{-1}$ ,  $1085\text{ cm}^{-1}$ ,  $1050\text{ cm}^{-1}$ ,  $940\text{ cm}^{-1}$ ,  $860\text{ cm}^{-1}$ ,  $745\text{ cm}^{-1}$ ,  $605\text{ cm}^{-1}$ ,  $510\text{ cm}^{-1}$ , and  $450\text{ cm}^{-1}$ . The assignment of the absorption bands of these glass–ceramics of the  $Li_2O$ – $Li_2MoO_4$ – $TiO_2$ – $P_2O_5$  system was done according to our previous work, interested in studying the glassy structure of this system [18]. The band positions and their assignments are listed in Table 4. The broad weak band at position  $1275\text{ cm}^{-1}$  is described to the asymmetric vibration of the  $P=O$  bond [ $\nu_{as}(P=O)$ ] and/or  $\nu_{as}(PO_2^-)$ , in the metaphosphate  $Q^2$  units, while the band at  $1120\text{ cm}^{-1}$  is attributed to symmetric stretching vibration in the  $\nu_s(PO_2^-)$  bond in  $Q^2$  chains. The strong band situated at  $1085\text{ cm}^{-1}$  is associated with asymmetric stretching modes of the  $\nu_{as}(PO_3)^{2-}$ , in pyrophosphate  $Q^1$  units, whereas the weak band at  $1025\text{ cm}^{-1}$  is identified with the



**Table 3** Crystal dimensions determined from Scherrer analyses

Diffraction peak	Crystalline phase	Composition (mol%)	Crystal size(nm)
1 0 1	Li <sub>2</sub> WO <sub>4</sub>	0	18
		5	18
		8	18
		10	18
		15	18
0 0 2	Li <sub>4</sub> P <sub>2</sub> O <sub>7</sub>	0	26
		5	26
		8	26
		10	26
		15	26



**Fig. 9** FTIR spectra of the crystallized glasses at 550 °C for 12 h

symmetric stretching modes of the pyrophosphate (PO<sub>3</sub>)<sup>2-</sup> units. The low shoulder band situated at the position 9040 cm<sup>-1</sup> is ascribed with the orthophosphate PO<sub>4</sub><sup>3-</sup> units. The bands at 860 cm<sup>-1</sup> are attributed to the asymmetric vibration modes of the P–O–P and/or P–O–M (M = W, Ti) bonds. The band at 745 cm<sup>-1</sup> is attributed to the symmetric stretching vibrations of the P–O–P ν<sub>s</sub>(P–O–P) bond, of bridging oxygen atoms. The band about 605 cm<sup>-1</sup> is associated with the symmetric vibration of the P–O–P bond in the Q<sup>2</sup> units. The broad bands in the 510–450 cm<sup>-1</sup> range belong to the deformation mode of the PO<sub>4</sub> units of phosphate glasses. In comparison, between

**Table 4** IR band assignments in the 1400–400 cm<sup>-1</sup> range frequency for the studied phosphate glasses

Position of band (cm <sup>-1</sup> )	Band assignment
1275	ν <sub>as</sub> (P = O)/ν <sub>as</sub> (PO <sub>2</sub> <sup>-</sup> )
1120	ν <sub>s</sub> (PO <sub>2</sub> ) <sup>-</sup>
1085	ν <sub>as</sub> (PO <sub>3</sub> ) <sup>2-</sup>
1050	ν <sub>s</sub> (PO <sub>4</sub> ) <sup>3-</sup>
940	ν <sub>as</sub> (P–O–P)/ν <sub>as</sub> (P–O–M) (M = W, Ti)
860	MO <sub>6</sub> (M = W, Ti)
745	ν <sub>s</sub> (P–O–P)
605	ν <sub>s</sub> (M–O–M) (M = W, Ti)
510–450	δ δ(O–P–O) and translation of cations

IR band assignments of the glasses and their glass–ceramics, we conclude that the structure of these materials (glasses and glass–ceramics) is mainly formed from the bonds of the phosphate units: metaphosphate PO<sub>2</sub><sup>-</sup> units, pyrophosphate PO<sub>3</sub><sup>2-</sup> units, and orthophosphate PO<sub>4</sub><sup>3-</sup> units.

At the substitution of the Li<sub>2</sub>WO<sub>4</sub> by TiO<sub>2</sub> in the glasses and their glass–ceramics, the band positions and their intensities have changed. We attributed these changes to the interaction between (50 – x)Li<sub>2</sub>O with xTiO<sub>2</sub> or/and (50 – x)WO<sub>3</sub> with xTiO<sub>2</sub>. But, for the glass–ceramics, the changes are due to the bonds breaking as a result of heat treatment to format crystalline phases: Li<sub>2</sub>WO<sub>4</sub> and Li<sub>4</sub>P<sub>2</sub>O<sub>7</sub> (see the section of the X-ray diffraction of glass–ceramics). Existing the tungsten into structural phosphates, well the IR spectra show bands attributed to WO<sub>4</sub> (725 cm<sup>-1</sup>) and WO<sub>6</sub> (920 cm<sup>-1</sup>) units [46]. At high TiO<sub>2</sub> content, the intensities of the bands at 1000 cm<sup>-1</sup> are associated with PO<sub>4</sub><sup>3-</sup> units and TiO<sub>4</sub> units, decreasing with slightly shifting towards higher wavenumber. Additionally, an increase of

TiO<sub>2</sub> content in the glasses leads to increasing the intensity of bands associated with the metaphosphate (PO<sub>2</sub>)<sup>-</sup> units. But the intensity of bands attributed to the pyrophosphate (PO<sub>3</sub>)<sup>2-</sup> groups decreased [18]. In contrary, at low TiO<sub>2</sub> content in glass–ceramics (from  $x = 8$  to  $x = 0$  mol%), it observed changes in form and intensity of bands, especially the bands range in 1247–1000 cm<sup>-1</sup>. These changes are associated with the precipitation of the crystalline phases (Li<sub>2</sub>WO<sub>4</sub> and Li<sub>4</sub>P<sub>2</sub>O<sub>7</sub>) in the heat-treated glasses. But, for the composition  $x = 10$  mol% and  $x = 15$  mol% of heat-treated glasses, it observed no change in form or intensity. Therefore, it assumed that the P–O–M (M = P, W) bonds are interrupted by the presence of the LiO<sub>2</sub>, then formation of new P–O–Ti bonds [47]. As a result of increasing, the P–O–Ti bonds in glasses lead to increasing of hardness of the glassy structure. Therefore, the formation of new crystalline phases contain titanium that needs more temperature and/or time for heat treatment of the glasses.

In conclusion, the IR spectra of the glass–ceramics show nearly the same IR vibrational modes as their parent glasses. The IR spectra of the glass–ceramics reveal a few sharp peaks in the far IR region and the mid-region spectrum. Due to the stretching of main phosphate network groups, it appears lower in the intensity of the vibrational bands. These results confirm that the crystalline phases separated, while the X-ray data indicated that the formation of these new crystalline phases (Li<sub>2</sub>WO<sub>4</sub> and Li<sub>4</sub>P<sub>2</sub>O<sub>7</sub>), which are suggested to be somewhat compacted or limited to two crystalline phases.

## 4 Conclusions

The Raman spectra of the prepared glasses show a conversion of metaphosphate units into pyrophosphate and orthophosphate units during the substitution of Li<sub>2</sub>WO<sub>4</sub> by TiO<sub>2</sub>. Crystallization kinetics of glasses is reported by DSC. Therefore, the activation energy of crystallization ( $E_c$ ) depends on the chemical composition of the glass ( $x = 5$  mol%), where its value is around  $\approx 184.482$  kJ/mol, while the obtained value of the parameter Avrami ( $n$ ) is about  $\approx 1.7$ , where it allowed us to predict that the crystallization of the glasses takes place according to a surface mechanism. In addition, the formation of the crystalline phases depends on the temperature and heat treatment time. Glass–ceramics obtained

from the studied glasses submitted to heating at two different durations were exploited by XRD and FTIR, whereas the crystallized phases (Li<sub>2</sub>WO<sub>4</sub> and Li<sub>4</sub>P<sub>2</sub>O<sub>7</sub>) into prepared glasses depend on the composition and the conditions of treatment. Also, X-ray patterns of crystalline phases are investigated to determine the crystal size for each crystallized phase into heat-treated glasses, where it found that the  $D_{(Li_2WO_4)} = 18$  nm and  $D_{(Li_4P_2O_7)} = 26$  nm. Furthermore, the crystal size of these crystalline phases was fixed with the variation of TiO<sub>2</sub> mol%. FTIR analysis has shown that the absorption bands of both spectra (glasses and glass–ceramics) were presented the same bands with quite different. Also, the results of the IR analysis confirmed the formation of the crystalline phases have been identified by X-ray diffraction. In the perspective work, we will focus on the study the electrical conduction mechanism into these glass–ceramics.

## Acknowledgements

The authors are grateful to G. Bánhegyi (Medicontur Medical Engineering Ltd., Herceghalmi út 1, Zsám-bék 2072, Hungary) for his comments and valuable suggestions.

## Author contributions

HE-S: Conceptualization, Writing—review & editing. LB: Supervision. ARFL: Visualization. AEB: Visualization. BM: Investigation. SH: Visualization.

## Declarations

**Conflict of interest** The authors declare no competing interests.

## References

1. T. Ishiyama, S. Suzuki, J. Nishii, T. Yamashita, H. Kawazoe, T. Omata, *Solid State Ionics* **262**, 856–859 (2014). <https://doi.org/10.1016/j.ssi.2013.10.055>
2. S. Hussain, X. Yang, M.K. Aslam, A. Shaheen, M.S. Javed, N. Aslam et al., *Chem. Eng. J.* **391**, 123595 (2020). <https://doi.org/10.1016/j.cej.2019.123595>
3. F. Zheng, M. Kotobuki, S. Song, M.O. Lai, L. Lu, J. Power Sources **389**, 198–213 (2018). <https://doi.org/10.1016/j.jpowsour.2018.04.022>

4. T. Minami, A. Hayashi, M. Tatsumisago, *Solid State Ionics* **177**, 2715–2720 (2006). <https://doi.org/10.1016/j.ssi.2006.07.017>
5. V.I. Voronin, E.a. Sherstobitova, V.a. Blatov, G.S. Shekhtman, *J. Solid State Chem.* **211**, 170–175 (2014). <https://doi.org/10.1016/j.jssc.2013.12.015>
6. E. Kartini, M. Nakamura, M. Arai, Y. Inamura, K. Nakajima, T. Maksum et al., *Solid State Ionics* **262**, 833–836 (2014). <https://doi.org/10.1016/j.ssi.2013.12.041>
7. T. Minami, *J. Non-Cryst. Solids* **73**(1–3), 273–284 (1985). [https://doi.org/10.1016/0022-3093\(85\)90353-9](https://doi.org/10.1016/0022-3093(85)90353-9)
8. P. Knauth, *Solid State Ionics* **180**(14–16), 911–916 (2009). <https://doi.org/10.1016/j.ssi.2009.03.022>
9. M. Tatsumisago, *Solid State Ionics* **175**(1–4), 13–18 (2004). <https://doi.org/10.1016/j.ssi.2004.09.012>
10. K. Minami, F. Mizuno, A. Hayashi, M. Tatsumisago, *Solid State Ionics* **178**(11–12), 837–841 (2007). <https://doi.org/10.1016/j.ssi.2007.03.001>
11. A.D. Robertson, A.R. West, A.G. Ritchie, *Solid State Ionics* **104**(1–2), 1–11 (1997). [https://doi.org/10.1016/S0167-2738\(97\)00429-3](https://doi.org/10.1016/S0167-2738(97)00429-3)
12. G.L. Henriksen, D.R. Vissers, *Journal of power sources* **51**(1–2), 115–128 (1994). [https://doi.org/10.1016/0378-7753\(94\)01965-7](https://doi.org/10.1016/0378-7753(94)01965-7)
13. S. Soman, Y. Iwai, J. Kawamura, A. Kulkarni, *J. Solid State Electrochem.* **16**(5), 1761–1766 (2012). <https://doi.org/10.1007/s10008-011-1592-4>
14. M. Tatsumisago, Y. Shinkuma, T. Minami, *Nature* **354**(6350), 217–218 (1991). <https://doi.org/10.1038/354217a0>
15. E. Kartini, V. Yapriadi, H. Jodi, M. Manawan, C. Panghegar, *Prog. Nat. Sci. Mater. Int.* (2020). <https://doi.org/10.1016/j.pnsc.2020.01.020>
16. H. Horiuchi, N. Morimoto, S. Yamaoka, *J. Solid State Chem.* **33**(1), 115–119 (1980). [https://doi.org/10.1016/0022-4596\(80\)90554-X](https://doi.org/10.1016/0022-4596(80)90554-X)
17. D.M.M. Krishantha, R.M.G. Rajapakse, D.T.B. Tennakoon, H.V.R. Dias, *J. Compos. Mater.* **40**(11), 1009–1021 (2006). <https://doi.org/10.1177/0021998305056388>
18. H. Es-Soufi, L. Bih, B. Manoun, P. Lazor, *J. Non-Cryst. Solids* **463**, 12–18 (2017). <https://doi.org/10.1016/j.jnoncrysol.2017.02.013>
19. M.A. Sayed, A.M. Ali, A. El-Rehim, A.F. Wahab, E. A., & K.S. Shaaban, *J. Electron. Mater.* (2021). <https://doi.org/10.1007/s11664-021-08921-9>
20. S.F. Ismail, M.R. Sahar, S.K. Ghoshal, *Mater. Res. Bull.* **74**, 502–506 (2016). <https://doi.org/10.1016/j.materresbull.2015.11.022>
21. K.S. Rao, M.S. Reddy, V.R. Kumar, N. Veeraiah, *Mater. Chem. Phys.* **111**(2–3), 283–292 (2008). <https://doi.org/10.1016/j.matchemphys.2008.04.012>
22. G.K. Marasinghe, M. Karabulut, C.S. Ray, D.E. Day, P.G. Allen, J.J. Bucher et al., *Ceram. Trans.* **93**, 195–202 (2003)
23. X. Fang, C.S. Ray, A. Mognuš-Milanković, D.E. Day, *J. Non-cryst. Solids* **283**(1–3), 162–172 (2001). [https://doi.org/10.1016/S0022-3093\(01\)00416-1](https://doi.org/10.1016/S0022-3093(01)00416-1)
24. G.M. Krishna, B.A. Kumari, M.S. Reddy, N. Veeraiah, *J. Solid State Chem.* **180**(10), 2747–2755 (2007). <https://doi.org/10.1016/j.jssc.2007.07.025>
25. M. Nagarjuna, T. Satyanarayana, Y. Gandhi, N. Veeraiah, *J. Alloys Compd.* **479**(1–2), 549–556 (2009). <https://doi.org/10.1016/j.jallcom.2008.12.132>
26. F. Delahaye-Carrière (1997). (Doctoral dissertation, Compiègne)
27. H. Es-Soufi, L. Bih, *J. Non-Cryst. Solids* **558**, 120655 (2021). <https://doi.org/10.1016/j.jnoncrysol.2021.120655>
28. A. El Hadrami, M. Mesnaoui, M. Maazaz, J.J. Videau, *J. Non-cryst. Solids* **331**(1–3), 228–239 (2003). <https://doi.org/10.1016/j.jnoncrysol.2003.08.066>
29. L. Ma, R.K. Brow, M.E. Schlesinger, *J. Non-Cryst. Solids* **463**, 90–101 (2017). <https://doi.org/10.1016/j.jnoncrysol.2017.02.022>
30. X. Li, Z. Xiao, M. Luo, X. Dong, T. Du, Y. Wang, *J. Non-Cryst. Solids* **469**, 62–69 (2017). <https://doi.org/10.1016/j.jnoncrysol.2017.04.023>
31. L. Ma, R.K. Brow, L. Ghussn, M.E. Schlesinger, *J. Non-Cryst. Solids* **409**, 131–138 (2015). <https://doi.org/10.1016/j.jnoncrysol.2014.11.019>
32. P.P. Poluektov, O.V. Schmidt, V.A. Kascheev, M.I. Ojovan, *J. Nucl. Mater.* **484**, 357–366 (2017). <https://doi.org/10.1016/j.jnucmat.2016.10.033>
33. H.E. Kissinger, *J. Res. Nat. Bur. Stand.* **57**, 217 (1956)
34. J.A. Augis, J.E. Bennett, *J. Therm. Anal.* **13**(2), 283–292 (1978). <https://doi.org/10.1007/BF01912301>
35. D.R. Lide (ed.), *CRC Handbook of Chemistry and Physics* (CRC Press, Boca Raton, 2001)
36. M. Avrami, *J. Chem. Phys.* **7**(12), 1103–1112 (1939). <https://doi.org/10.1063/1.1750380>
37. M. Avrami, *J. Chem. Phys.* **8**(2), 212–224 (1940). <https://doi.org/10.1063/1.1750631>
38. M. Avrami, *J. Chem. Phys.* **9**, 177–184 (1941). <https://doi.org/10.1063/1.1750872>
39. E.C. Cardillo, S. Teryn, C. Lopez, G. Narda, M.A. Frechero, *Ceram. Int.* (2020). <https://doi.org/10.1016/j.ceramint.2020.05.168>
40. E. Haily, L. Bih, A. El Bouari, A. Lahmar, M. El Marssi, B. Manoun, *Phase Transit.* (2020). <https://doi.org/10.1080/01411594.2020.1837369>
41. F.H. ElBatal, M.A. Marzouk, H.A. ElBatal, *J. Mol. Struct.* **1121**, 54–59 (2016). <https://doi.org/10.1016/j.molstruc.2016.05.052>

42. H. Horiuchi, N. Morimoto, S. Yamaoka, *J. Solid State Chem.* **33**(1), 115–119 (1980)
43. P. Scherrer, *Nachr. Ges. Wiss. Göttingen* **2**, 98–100 (1918)
44. J.I. Langford, A.J.C. Wilson, *J. Appl. Cryst.* **11**, 102–113 (1978)
45. D.J. Lim, N.A. Marks, M.R. Rowles, *Carbon* **162**, 475–480 (2020). <https://doi.org/10.1016/j.carbon.2020.02.064>
46. L. Koudelka, O. Kupetska, P. Kalenda, P. Mošner, L. Montagne, B. Revel, *J. Non-Cryst. Solids* **500**, 42–48 (2018). <https://doi.org/10.1016/j.jnoncrysol.2018.05.028>
47. M. Azmoonfar, M.H. Hekmat-Shoar, M. Mirzayi, *Ionics* **15**(4), 513–518 (2009). <https://doi.org/10.1007/s11581-008-0299-8>

**Publisher's Note** Springer Nature remains neutral with regard to jurisdictional claims in published maps and institutional affiliations.